Tau Paired Helical Filaments from Alzheimer's Disease Brain and Assembled in Vitro Are Based on β-Structure in the Core Domain†

Stefan Barghorn,‡ Peter Davies,§ and Eckhard Mandelkow*,‡

Max-Planck-Unit for Structural Molecular Biology, Notkestrasse 85, 22607 Hamburg, Germany, and Department of Pathology and Neuroscience, Albert Einstein College of Medicine, 1300 Morris Park Avenue, Bronx, New York 10416

Received September 19, 2003; Revised Manuscript Received November 27, 2003

ABSTRACT: Tau protein, a neuronal microtubule-associated protein, forms insoluble fibers ("paired helical filaments") in Alzheimer's disease and other tauopathies. Conflicting views on the structure of the fibers have been proposed recently, ranging from mainly α-helical structure to mainly β-sheet, or a mixture of mostly random coil and β-sheet. We have addressed this issue by studying tau fibers immunopurified from Alzheimer brain tissue by a conformation-specific antibody and comparing them with fibers reassembled from recombinant tau or tau constructs in vitro, using a combination of electron microscopy and spectroscopic methods. Brain-derived fibers and reassembled fibers both exhibit a typical twisted appearance when examined by electron microscopy. The soluble tau protein is a natively unfolded protein dominated by random coil structure, whereas Alzheimer PHFs and reassembled fibers show a shift toward an increase in the level of β-structure. The results support a model in which the repeat domain of tau (which lies within the core of PHFs) adopts an increasing level of β-structure during aggregation, whereas the N- and C-terminal domains projecting away from the PHF core are mostly random coil.

Pathological protein aggregates lie at the root of a number of human diseases, including sickle cell anemia (hemoglobin), systemic amyloidosis (transthyretin), or degenerative brain diseases such as Alzheimer's disease, Parkinson's disease, and Creutzfeld-Jacob disease (Aβ peptide and tau protein, α-synuclein, or prion protein, respectively). They involve diverse proteins, and there may be multiple causes of their abnormal aggregation; however, there is a general consensus that preventing or retarding the aggregation process would be a major step toward curing the diseases. This calls for a detailed investigation of the structural and biochemical requirements of aggregation. In some cases, the subunit proteins are globular proteins, which switch from their normal oligomeric state to a fibrous polymeric state due to mutations which alter their interactions (e.g., hemoglobin S and transthyretin). In other cases, the proteins may be partly unfolded, exposing novel surfaces for unfavorable interactions. These interactions are often centered around regions prone to forming β-structure because this leads to highly stable aggregates that are not easily removed by the cell's defense mechanism (protein degradation by the proteasome). Such fibers rich in β-structure tend to bind certain dyes (e.g., congo red and thioflavine S) and have therefore been termed "amyloid" (*1*).

Alzheimer's disease, the leading dementia in the elderly population, is characterized by two types of pathological protein deposits, the Alzheimer amyloid fibers consisting of the Aβ peptide (leading to the amyloid plaques) and fibers of tau protein [leading to neurofibrillary tangles (NFTs)]. The Aβ peptide has a partially hydrophobic character and a strong propensity for β-structure, both of which promote aggregation, and therefore, the building principles of Aβ fibers are generally accepted, even though the structural details are still under investigation (*2*−*5*). By contrast, the building principles of tau fibers are less clear and still a matter of debate. The CD[1] spectrum of tau is dominated by a random coil pattern, consistent with the unusually high solubility and hydrophilic composition of tau, which provides no obvious clues about folding or aggregation (*6*−*8*). Some short peptides derived from the tau sequence can adopt an α-helical conformation, but only in nonphysiological buffers including helix-inducing agents (*9*−*12*). X-ray patterns of NFTs or reassembled tau fibers show only weak or no contributions from β-structure (*8*, *13*). NFTs and tau fibers stain poorly with congo red, a dye considered to be indicative of cross-β-structure, compared with thioflavine S (*14*). Until some years ago, the investigation of the secondary structure of tau PHFs has been confounded by the difficulty of identifying conditions for assembling tau in vitro into bona fide PHFs resembling those of Alzheimer's disease. This difficulty can now be overcome with the help of certain cofactors (polyanions in the form of peptides, nucleic acids, carbohydrates, or fatty acids), by using truncated constructs of tau (e.g., the repeat domain) or variants with mutations that occur in frontotemporal dementias (e.g., ΔK280 and P301L) (*15*−*20*). The results suggest that the repeat domain

† This work was supported in part by the Deutsche Forschungsgemeinschaft (DFG).

* To whom correspondence should be addressed. Telephone: +49-40-89982810. E-mail: mand@mpasmb.desy.de or davies@aecom.yu.edu.

‡ Max-Planck-Unit for Structural Molecular Biology.

§ Albert Einstein College of Medicine.

[1] Abbreviations: CD, circular dichroism; DTT, dithiothreitol; FTDP-17, frontotemporal dementia and parkinsonism linked to chromosome 17; FTIR, Fourier transform infrared; PBS, phosphate-buffered saline; PHF, paired helical filaments.

10.1021/bi0357006 CCC: $27.50
Published on Web 01/16/2004

of tau is sufficient for forming PHFs and therefore contains the building principle, consistent with the observation that the repeat domain represents the core of Alzheimer PHFs (*21*, *22*). The aggregation in vitro is accompanied by a partial transition from random coil to β-structure, centered around hexapeptide motifs in the second or third repeat (*20*, *23*−*26*).

There remains the question of whether the conclusions from in vitro experiments can be applied to tau aggregates in Alzheimer brains. To address this issue, one must isolate fibers from Alzheimer brain and study them by methods revealing secondary structure. Using this approach, three recent publications arrived at conflicting conclusions. Sadqi et al. (*27*) isolated Alzheimer PHFs by the method of Greenberg and Davies (*28*), studied them by spectroscopy (CD and FTIR), and claimed that an almost entirely α-helical structure existed. Goux (*29*) used PHFs prepared from Alzheimer brains by immunopurification (*30*, *31*), applied spectroscopic methods (CD), and claimed that partly α-helical, β-sheet, and turn structure existed, depending on buffer conditions. Berriman et al. (*32*) used PHFs from Down's syndrome brains and studied them by selected area electron diffraction; they also studied PHFs reassembled in vitro by FTIR and found predominantly cross-β-structure in both cases. Our own previous results on PHFs made from recombinant tau (*23*, *24*) were in general agreement with those of Berriman et al. (*32*), namely, a PHF core formed from the repeat domain which is partially folded into a cross-β-structure, embedded in a largely unstructured "fuzzy coat". However, because of the divergent published results, we decided to reinvestigate the question of Alzheimer-derived PHF structure. In the study presented here, we used immunopurified PHFs, prepared as described previously (*30*, *31*). The isolation is based on the reaction of Alzheimer tau fibers with a conformation-dependent antibody (MC-1) and therefore generates PHFs that are more pure than those generated by the Greenberg−Davies method (*28*), which is based on solubility in sarkosyl buffer. We conclude that Alzheimer PHFs are based on β-structure embedded in an environment of unstructured protein, but we find no measurable indications of α-helical structure. Thus, tau fibers can be classified as "amyloid" in a broad sense.

MATERIALS AND METHODS

Chemicals and Proteins. The human tau isoforms and tau constructs (see Figure 1) were expressed in *Escherichia coli* as described previously (*33*). The numbering of the amino acids is that of the isoform htau40 which contains 441 residues (*34*). The protein was expressed and purified as described previously (*35*), making use of the heat stability and FPLC Mono S chromatography with subsequent gel filtration (Superdex200 for tau isoforms and Superdex75 for tau constructs, Amersham Biosciences, Freiburg, Germany). The elution profiles from the columns were calibrated by a set of standard globular proteins [thyroglobulin (669 kDa), ferritin (440 kDa), catalase (232 kDa), aldolase (158 kDa), albumin (67 kDa), ovalbumin (43 kDa), chymotrypsinogen (25 kDa), and ribonuclease A (13.7 kDa)] which are available in the high- and low-molecular weight gel filtration calibration kit from Amersham Biosciences. The purity of the proteins was analyzed by SDS−PAGE. Protein concentrations were determined by the Bradford assay or by UV absorption at 214 nm against a BSA standard curve.

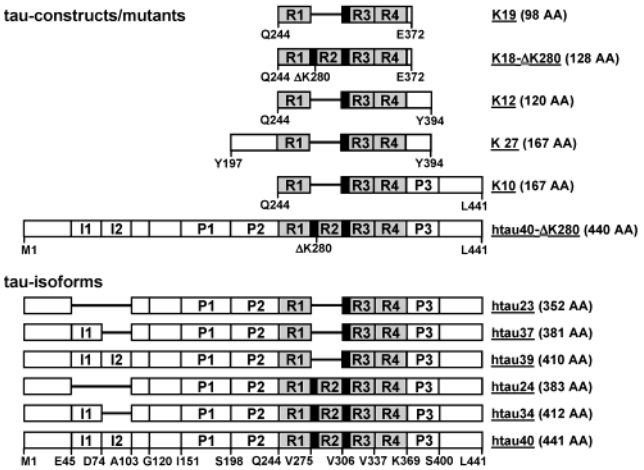

FIGURE 1: Diagram of human tau isoforms, mutants, and constructs. The bottom bar shows the longest tau isoform htau40 (441 amino acids) in the CNS. The C-terminal half of tau contains three or four pseudorepeats (∼31 residues each, R1−R4, gray) which together with their proline-rich flanking regions (P) constitute the microtubule-binding domain. Repeat R2 and the two near N-terminal inserts (I1 and I2) may be absent due to alternative splicing, as in htau23, the shortest human isoform (352 amino acids). Hexapeptide motifs PHF6* (^{275}VQIINK^{280}) and PHF6 (^{306}VQIVYK^{311}) at the beginning of R2 and R3 (black) are important for PHF formation because they induce β-structure. Construct K18 comprises only the four repeats (R1−R4), and constructs K19, K12, K27, and K10 comprise only three repeats (R1, R3, and R4) with varying N- and C-terminal extensions. The mutant htau40-ΔK280 occurs in FTDP-17; this mutation was also introduced into some four-repeat constructs such as K18-ΔK280.

PHFs Reassembled in Vitro. The aggregation of tau into PHFs was induced by incubating varying concentrations of tau isoforms or tau constructs (typically in the range of 5−50 μM) in volumes of 20−2000 μL at 37 °C in PBS (pH 7.4) with 1 mM DTT and mixing it with the anionic cofactor heparin (MW ≈ 6000 Da, used in a tau:heparin molar ratio of 4:1). Incubation times for filament formation varied from hours up to several days. PHF aggregation was checked by electron microscopy and thioflavine S fluorescence (*36*).

Alzheimer PHFs. Immunoaffinity-purified PHFs were prepared from three Alzheimer's disease brains as described previously, using the reaction with the MC-1 antibody (*30*, *31*). The Alzheimer PHFs were concentrated by being pelleted at 86000*g* for 14 h and resuspended in PBS. The purity of the PHF preparation was analyzed by SDS−PAGE and Western blotting with the rabbit polyclonal pan-tau antibody K9JA (Dako Diagnostics, Hamburg, Germany) raised against the four repeats and the C-terminal tail of tau.

Electron Microscopy. To confirm PHF assembly in vitro and to examine the overall appearance of Alzheimer PHFs, 10 μL protein solutions diluted to 1−10 μM protein were placed on 600-mesh carbon-coated copper grids for 45 s, washed twice with H_2O, and negatively stained with 2% uranyl acetate for 45 s. The specimens were examined with a Philips CM12 electron microscope at 100 kV.

Fourier Transform Infrared Spectroscopy. FTIR experiments were performed on a Jasco FTIR-410 instrument (Jasco, Gross-Umstadt, Germany). Atmospheric water vapor was removed by flushing the spectrometer with nitrogen. Interferograms were recorded between 1700 and 1600 cm^{-1},

and 128 spectra were averaged. They were acquired in the transition mode using CaF_2 cells separated by spacers of 25 μm. After a reference spectrum of the instrument and of the fresh D_2O lot that was used was recorded, the protein solutions were applied, and the absorbance spectrum of the sample was measured. The D_2O spectra and sample spectra were first corrected for the water vapor background before subtracting the D_2O spectra from the sample spectrum. To facilitate comparison, the spectra were then normalized with respect to their maxima. Typical concentrations [measured by absorption at 214 nm (A_{214})] were 3−6 mg/mL (70−600 μM, depending on the tau construct and tau isoform) for soluble tau protein and for reassembled or brain-derived PHFs.

Circular Dichroism Spectroscopy. All measurements were carried out with a Jasco J-715 CD spectrometer in a cuvette with a path length of 0.05 cm. The scanning speed was 100 nm/min with a bandwidth of 1.0 nm and a response time of 0.5 s. In each experiment, 25 spectra were summed and averaged. To minimize the signal-to-noise ratio in the lower UV range, a second spectrum from each sample was recorded between 194 and 200 nm with a scanning speed of 20 nm/min at a bandwidth of 1.0 nm and a response time of 1.0 s. In this case, 100 spectra were summed and averaged. The two final spectra for each sample were then joined together using the CD software implemented "concatenate" function. For calculation of the mean residue ellipticity, the protein concentration was obtained by using the second channel of the CD spectrometer to measure the absorption of the protein sample at 214 nm (where absorption is dominated by the peptide bonds). Calibration of A_{214} was done by BSA standards. The secondary structure interpretation of the CD data was performed with the program Dicroprot (*37*) which allows fitting against standard CD spectra (*38*) as well as comparison with a set of known proteins.

RESULTS

Morphology and Composition of Immunopurified PHFs from Alzheimer Brain and PHFs Assembled in Vitro. To ensure that the tau fibers from AD brains and assembled in vitro were similar in overall morphology and composition, we compared them by electron microscopy, SDS gel electrophoresis, and Western blotting. PHFs from AD brains were obtained from three different Alzheimer cases, using immunoaffinity purification with the MC-1 antibody (*30*, *31*). In all cases, the filaments were mainly of the paired helical type, had a typical length of 100−500 nm, were 10−25 nm wide, and had a crossover repeat of ~80 nm (Figure 2, top panel). Thus, they showed all characteristics of "Alzheimer PHFs" (*39*, *40*). The samples were subsequently pelleted and resuspended in PBS to increase the concentration for the structural analysis. This step did not change their overall morphology (Figure 2, middle panel). By contrast, in vitro assembly of PHFs was done using recombinant four-repeat and three-repeat tau constructs (K18 and K19, respectively) and the longest tau isoform htau40 as described previously (*23*, *41*). The four-repeat construct K18 and full-length htau40 contained the second repeat R2 (exon 10) and were used as mutants lacking lysine 280 (ΔK280), resembling a naturally occurring mutation in FTDP-17 (*42*). This mutation leads to an increased level of PHF formation and a very regular paired helical appearance of the filaments (*20*, *23*, *41*). The in vitro PHFs were somewhat longer, but otherwise exhibited the same characteristics (Figure 2, bottom panel).

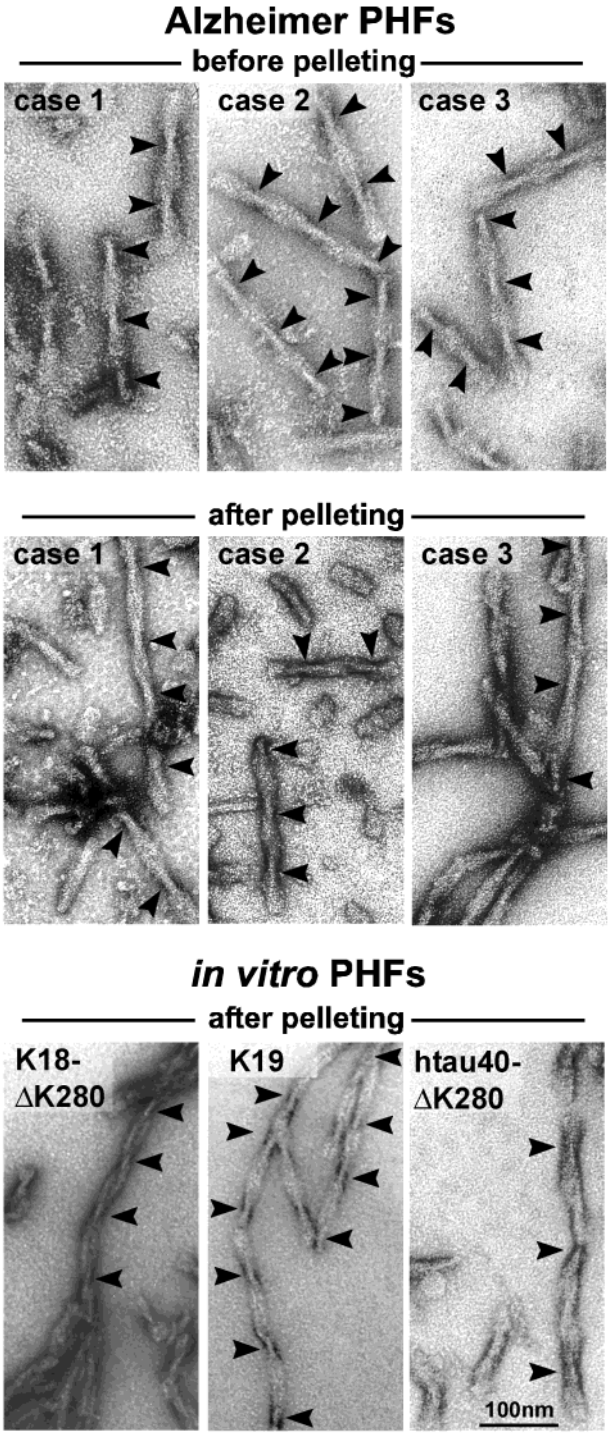

FIGURE 2: Negative stain electron microscopy of PHFs isolated from Alzheimer brain and in vitro polymerized PHFs: PHFs extracted from three individual Alzheimer disease brains directly after immunoaffinity purification (top panel), PHFs from the three individual Alzheimer disease brains after subsequent pelleting to further purify and concentrate the sample for the following experiments (middle panel), and PHFs reassembled from recombinant tau in vitro (after pelleting) in the presence of the polyanionic cofactor heparin (bottom panel). Most fibers exhibit the characteristics typical of brain-derived Alzheimer PHFs with a paired helical appearance, a width of 10−25 nm, and a crossover repeat of ~80 nm. The bar is 100 nm long.

In the SDS gel, the three individual Alzheimer PHFs all exhibited the typical three- to four-band appearance [bands

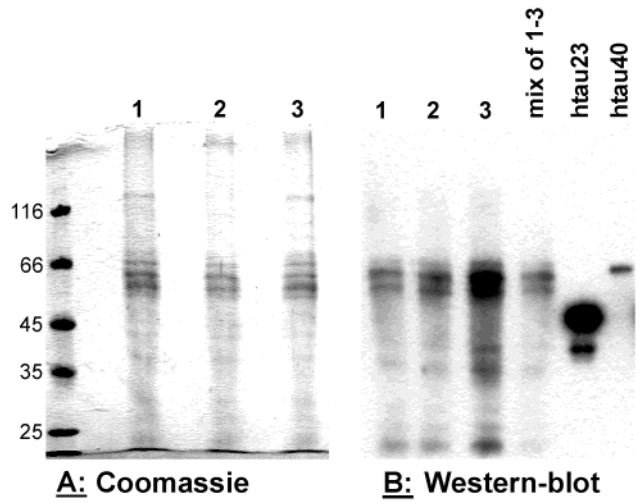

FIGURE 3: SDS−PAGE and Western blot analysis of Alzheimer PHFs. Three individual PHF preparations derived from different Alzheimer brains were investigated (lanes 1−3 in panels A and B). Prior to SDS−PAGE, the PHFs were dissolved by adding SDS−PAGE sample buffer and heating to 96 °C for 15 min. (A) The SDS−PAGE shows the triplet pattern characteristic of phosphorylated Alzheimer tau ($M_r \sim 55$, 64, and 69 kDa) and a minor fourth band (∼73 kDa) (*43*−*45*). Apart from these distinct bands due to intact tau isoforms, there are further bands and a diffuse smear mainly in the lower-M_r region due to tau fragments, together comprising roughly 75% of the total protein. (B) Western blotting of three individual cases and a mixture of all three Alzheimer PHF samples with the polyclonal pan-tau antibody K9JA shows that the three- to four-band pattern, the low-M_r smear, and part of the high-M_r smear are composed of tau protein. The control shows the shortest and longest tau isoform (htau23 and htau40, respectively).

at 55, 64, and 69 kDa and a minor fourth band (72−74 kDa) which contain the six human tau isoforms in a highly phosphorylated form (*43*−*45*)] (Figure 3A). In two Alzheimer cases (lanes 1 and 3 in Figure 3A), a further distinct band running just above the 116 kDa marker was present, and in all three cases, the typical broadly distributed smear at higher and lower M_r values was visible. In a Western blot analysis, the samples were probed with the polyclonal antibody K9JA that recognizes the repeat region and the C-terminus of tau. The pattern was comparable to that of the Coomassie-stained gel with regard to the three- to four-band pattern and the high- and low-M_r smear, showing that most of the protein (∼75% as measured by densitometric methods) in the Alzheimer PHF preparations was indeed tau (Figure 3B). This issue is important for interpreting the spectroscopic data to be described next.

CD Spectroscopy of Alzheimer PHFs and in Vitro Reassembled PHFs Reveal β-Structure Embedded in Random Coil Structure. Thus far, tau or tau aggregates have not been accessible to a high-resolution analysis by X-ray or NMR methods, and therefore, structural analyses must rely on spectroscopic approaches sensitive to secondary structure, primarily far-UV CD and FTIR. In both cases, there is considerable room for interpretation since the analysis is model-dependent; this is particularly true for natively unfolded proteins for which a database of crystal structures is not available (*46*, *47*). Nevertheless, some general features can be derived from the CD traces shown in Figure 4. All soluble tau proteins and constructs are dominated by "random coil" structure, consistent with earlier observations (*6*, *8*, *24*) [Figure 4A−C (dashed line)]. This is characterized by a

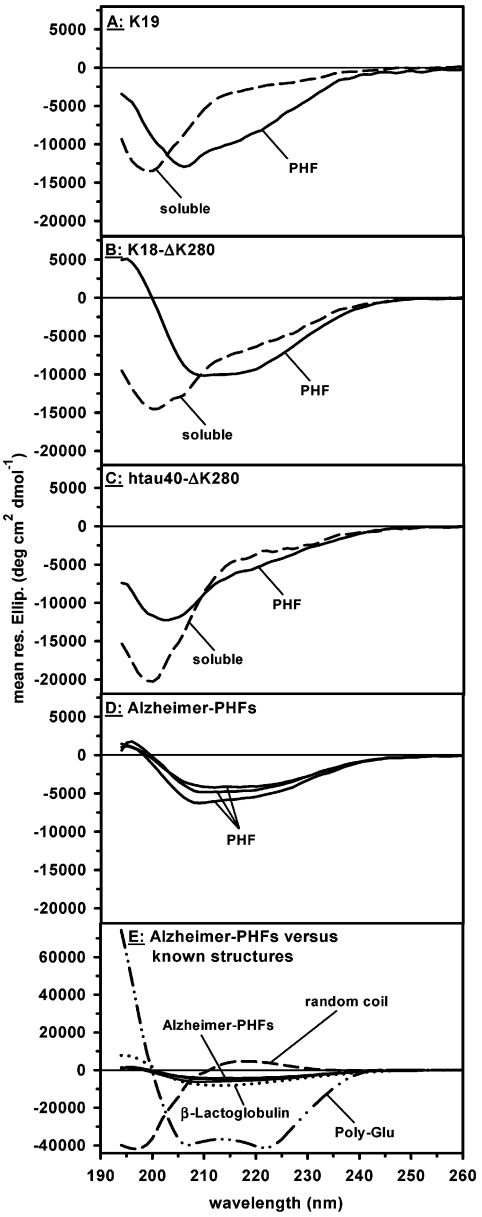

FIGURE 4: CD spectra of PHFs derived from Alzheimer brain, PHFs reassembled from recombinant tau, and soluble tau. The soluble proteins (dashed lines) of the three-repeat construct K19 (A), the four-repeat construct K18-ΔK280 (B), and the full-length isoform htau40-ΔK280 (C) exhibit typical random coil spectra. Upon filament formation (solid lines), the spectra change and show an increase in β-sheet content. This is most obvious with construct K18-ΔK280 (B) which carries an FTDP-17 mutation strongly favoring β-structure, the three-repeat construct K19 (A), and to a much lesser extent full-length htau40-ΔK280 (C). The Alzheimer PHF samples of three individual cases exhibit very similar spectra, indicating substantial β-sheet structure (D). In panel E, a comparison of the Alzheimer PHF spectra with spectra of proteins with known secondary structure is shown. Note that the spectra of Alzheimer PHFs resemble that of β-lactoglobulin, a protein consisting of ∼36% β-structure, ∼9% α-helix, and 55% coil (dotted line in panel E). By contrast, the α-helical spectrum [polyglutamic acid (dashed and dotted line), from the software program Dicroprot (*37*)] and the random coil spectrum (dashed line) can clearly be differentiated from the Alzheimer PHF spectra. Using the Greenfield−Fasman procedure, the fit of the PHF spectrum in panel B yields 17% α-helix, 31% β-sheet, and 52% others; the mean values for panel D are 8% α-helix, 18% β-sheet, and 74% others. The larger amplitude mostly accounts for the seemingly higher α-helix content in panel B (approximately −10000 in panel B and approximately −5000 in panel D).

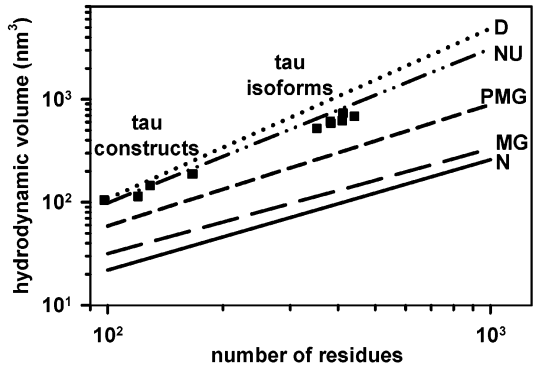

FIGURE 5: Hydrodynamic parameters of tau isoforms and constructs deduced from gel filtration. The six tau isoforms have Stokes radii of ~5−5.6 nm, corresponding to equivalent volumes of 520−680 nm³. The shorter tau constructs (K19, K18, K12, K27, and K10) comprising the microtubule binding repeat region with varying N- and C-terminal parts (see Figure 1) have Stokes radii of ~3−3.6 nm (V = 105−190 nm³). The values agree closely with the generalized dependence of V on the residue number derived from many natively unfolded proteins (NU) (*50*). For comparison, the plot also shows the dependence of volume on chain length n for natively folded proteins (N), molten globule states (MG), pre-molten globule states (PMG), and protein denatured by GuHCl (D) (lines replotted from ref *49*). Note that some data points for the tau isoforms and constructs are so close together that they cannot be distinguished in this graph.

negative peak around 200 nm (*38*, *48*). In particular, there is no major difference between the repeat domain (K18 and K19) and full-length tau, indicating that the microtubule-binding domain and the projection domain are similarly disordered in the unbound state. The mean residue ellipticity reaches values of around −15 to −20 × 10³, approximately half of the potential maximum (ca. −40 × 10³). This could mean that other unidentified secondary structure elements contribute, or (more likely) that the standard interpretation of CD curves based on model peptides or crystallized proteins cannot be fully applied to unfolded proteins such as tau (*49*).

The conclusions from the CD data are supported by the hydrodynamic behavior of tau, as determined by its elution from a gel filtration column (Amersham Superdex200 for tau isoforms and Superdex75 for tau constructs) calibrated with known proteins. For the six tau isoforms in the human CNS (containing 352−441 residues), the Stokes radii ranged from 5.0 to 5.6 nm; for constructs containing the repeats and adjacent regions (97−167 residues), the range was 2.9−3.5 nm (Figure 5). These values are much larger than expected for folded globular proteins and are in fact consistent with values expected of natively unfolded proteins (*49*, *50*), in agreement with our earlier solution X-ray results (*8*), and with the flexibility observed by NMR spectroscopy (*51*).

The CD spectra change when tau is induced to aggregate into PHFs. Figure 4A−C (solid lines) shows the PHF spectra after separation from soluble tau by a clearing spin. For three-repeat construct K19, the minimum shifts toward a higher wavelength, indicating a transition to a higher β-sheet content (Figure 4A). This change is even more pronounced for the FTDP-17 mutant of four-repeat construct K18 (K18-ΔK280, Figure 4B), consistent with the strong tendency of this mutant to form PHFs due to an increased propensity for β-sheet formation (*20*, *23*). For full-length tau, the shift in the spectrum toward a higher overall β-structure content is small (Figure 4C), indicating that the domains outside the repeats retain their unstructured state even after PHF aggregation. The data underscore the observations that the repeat domain forms the core of the PHFs (*21*, *22*), that the aggregation involves the generation of β-structure (*23*, *24*), and that the N- and C-terminal flanking domains remain largely as an unstructured "fuzzy coat".

The spectra of all immunopurified Alzheimer PHF samples are highly reproducible (Figure 4D). They show a broad trough between ~208 and 225 nm and a transition to positive values around 200 nm. These features are typical of a major contribution from β-structure combined with other disordered domains. This is illustrated by the good agreement with the CD spectrum of β-lactoglobulin [Figure 4E (dotted line)], a protein of known structure which contains ~36% β-sheet, ~9% α-helix, and ~55% random coil (*52*) (PDB entry 1BEB). Conversely, all spectra from Alzheimer PHFs are distinctly different from those of α-helical samples (see the example of poly-Glu in Figure 4E). A simple indicator for α-helix content is the ratio of ellipticities at 193 nm [high positive value, Figure 4E (dotted and dashed line)] and 222 nm (second negative peak); for typical α-helical structures, the ratio is approximately −2.5 and drops in proportion with a decrease in helix content (*53*, *54*). For the Alzheimer PHFs, the ratio varies between −0.25 and −0.55, confirming the low α-helical content.

It is interesting to note that the shapes of the Alzheimer PHF spectra closely resemble that of the polymerized K18-ΔK280 sample, except for a 2-fold smaller amplitude (compare the solid lines in panels B and D of Figure 4). One explanation would be that the concentration of the Alzheimer PHF sample, measured at a peptide bond concentration of 2.8−4.6 mM by the absorption at 214 nm, is overestimated ~2-fold. Alternatively, if the A_{214} value reflects the correct concentration, Alzheimer PHFs might contain conformations or even nonprotein components that cause the entire spectrum to be scaled down.

FTIR Spectroscopy Shows an Increased Level of β-Sheet Structure of PHFs. As a second method of monitoring the conformation of soluble tau and PHFs, we performed FTIR-spectroscopy (Figure 6). The method does not distinguish well between random coil and α-helical conformations, but it is sensitive to β-structure, which shifts the maximum to lower wavenumbers. Soluble proteins K19, K18-ΔK280, and full-length htau40-ΔK280 exhibit FTIR maxima around 1645−1646 cm^{-1}, consistent with the CD experiments and the dominance of the random coil conformation [Figure 6A−C (dashed lines)]. Upon PHF polymerization, the spectra of the repeat constructs shift the maximum to ~1629 and 1626 cm^{-1} [Figure 6A,B (solid lines)], indicating a shift toward a high β-structure content (*55*, *56*). In the case of PHFs from the full-length htau40-ΔK280, the shift is less pronounced, as expected since the β-forming repeat domain is embedded in the larger random coil flanking domains [Figure 6C (solid line)]. Note that construct K18-ΔK280 shows a slight shoulder around 1625 cm^{-1} already in the soluble state. This is due to the spontaneous tendency of this protein to oligomerize and to form β-structure even in the absence of polyanionic cofactors (*20*, *23*, *41*) and illustrates the sensitivity of FTIR.

Next we assessed the Alzheimer PHFs. Since FTIR requires a high concentration of protein (~2 mg/mL or higher

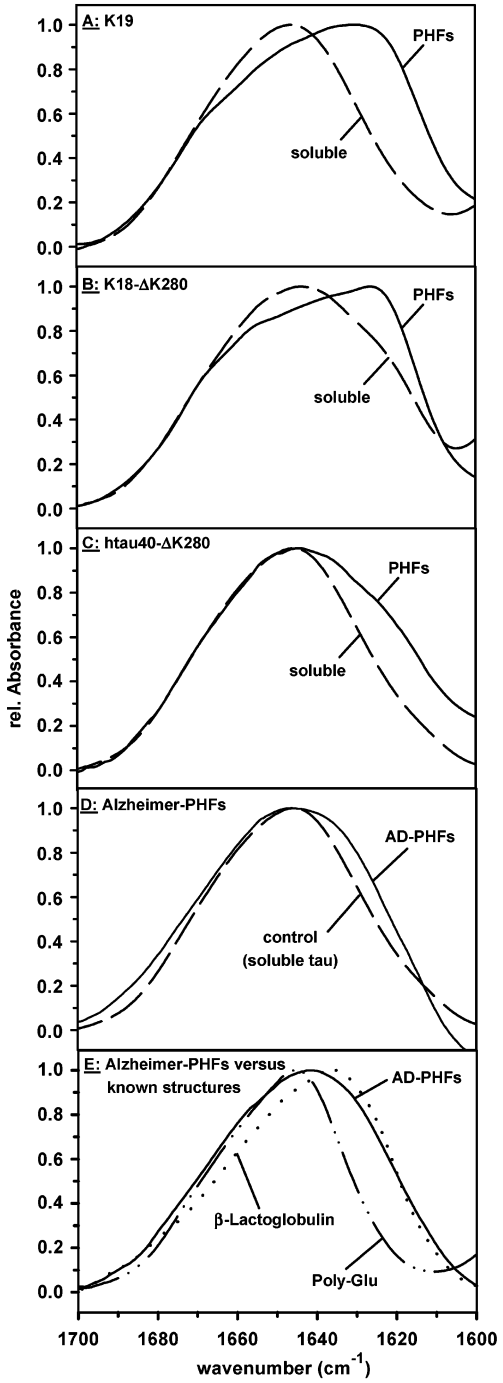

FIGURE 6: FTIR spectra of PHFs from Alzheimer brain tissue, PHFs reassembled from recombinant tau, and soluble recombinant tau: (A) three-repeat construct K19, (B) four-repeat construct K18-ΔK280, (C) full-length isoform htau40-ΔK280, and (D) AD-PHFs. Soluble recombinant tau (dashed lines) exhibits spectra with maxima at ~1645 cm^{-1}, indicating a random coil structure of the protein. By contrast, the corresponding spectra of PHFs reassembled in vitro from recombinant tau are shifted to the right (lower wavenumbers) with maxima or shoulders around 1630 cm^{-1} (solid lines in panels A−C), indicating an increase in the level of β-structure during PHF assembly. To measure the FTIR spectrum of the Alzheimer PHFs (D, solid line), three individual cases were pooled to increase the PHF concentration to ~3 mg/mL. The spectrum shows an additional shoulder around 1630 cm^{-1}, indicating an increased level of β-structure. (E) The spectrum of Alzheimer PHFs (solid line) resembles that of β-lactoglobulin [consisting of ~36% β-structure, ~9% α-helix, and 55% random coil (dotted line in panel E)] and can clearly be differentiated from the α-helical spectrum of polyglutamic acid (dashed and dotted line).

for reliable traces), we pooled three individual samples to obtain a high-quality FTIR spectrum at a tau concentration of ~3 mg/mL. In Figure 6D (dashed line), the spectrum of the soluble full-length htau40-ΔK280 with its maximum at 1646 cm^{-1} is shown for comparison. The spectrum of the Alzheimer PHFs has a maximum at 1645 cm^{-1} and exhibits an additional shoulder at lower wavenumbers [~1630 cm^{-1}, Figure 6D (solid line)]. Compared to the spectrum of β-lactoglobulin [~36% β-sheet, ~9% α-helix, and ~55% random coil, as determined by X-ray crystallography (PDB entry 1BEB); Figure 6E (dotted line)], the shoulder at 1630 cm^{-1} of the Alzheimer PHF spectrum is indicative of β-sheet structure. In contrast, the spectrum of poly-Glu [Figure 6E (dashed and dotted line)] is much narrower in the region around 1630 cm^{-1}. The fact that the maximum of the poly-Glu spectrum (1646 cm^{-1}) is comparable to that of the soluble tau protein [Figure 4D,E (dashed line)], which is comprised of a random coil structure, shows the poor distinction of α-helical and random coil structures by FTIR (*57*, *58*). Taken together, these results illustrate that bona fide Alzheimer PHFs contain β-structure in an overall random coil environment.

DISCUSSION

This study was performed to improve our understanding of the structure of tau and its pathological aggregation in Alzheimer's disease and related tauopathies. A clear grasp of the principles that govern the abnormal behavior of tau would help in the development of strategies against the disease process. For example, if tau could be considered a toxic amyloid because of its ability to interact via β-structure, it would make sense to search for "β-breaking" drugs; this approach is being pursued for other amyloids (*59*, *60*) as well as tau (*61*). Conversely, it is possible that other properties of tau are responsible for its toxicity, for example, its upregulation, mutation, or abnormal phosphorylation, as suggested by recent results from model organisms (*62*−*64*), so that other strategies of combating neurodegeneration would be more appropriate (*65*). In either case, it would be important to understand the principles that cause aggregation. In this regard, the current situation is not satisfactory because several recent publications contradict each other. To compare the different conclusions, we must consider separately the sources of protein, the methods used, and the interpretations.

In the case of soluble tau (recombinant or purified from brain), there is a consensus that it is best described as a natively unfolded, highly flexible protein whose CD, FTIR, X-ray, and NMR spectra or hydrodynamic behavior is dominated by the signatures of "random coil" (*6*, *8*, *15*, *24*, *51*). This is in agreement with the hydrophilic character of the sequence and tau's high solubility (*7*), and is evidenced by a negative maximum around 200 nm in the CD spectrum, a peak at ~1645 cm^{-1} in the amide I band of the FTIR spectrum, the absence of a defined radius of gyration by X-ray scattering (*8*, *15*, *23*, *24*), and unusually large Stokes radii [see Results (Figure 5)]. NMR studies of selected tau peptides confirm the absence of ordered secondary structure (except when α-helix is enforced by adding the α-helix inducer trifluoroethanol) (*9*−*12*). It should be kept in mind, however, that the absence of observable periodic structure does not necessarily mean total randomness of the protein. For example, it is interesting that the sequence of the ~20

C-terminal residues would be compatible with an amphiphilic α-helix which could interact with other domains of tau or partners of tau (*9*, *11*). The hexapeptide motifs in R2 and R3 (Figure 1) are predicted to form extended structure, ready to enter β-sheet interactions. Part of the proline-rich domains flanking the repeats might fold into a polyproline helix. However, these motifs are small in comparison with full-length tau and would not change the overall appearance of an unstructured protein.

Differences between published reports become apparent when tau filaments are considered. With respect to protein source and composition, we must distinguish at least three types of preparations.

(1) The first is filaments made in vitro from recombinant tau or tau domains (e.g., repeat domain). They have a well-defined composition (Figure 2), but they lack some of the modifications of Alzheimer PHFs, notably, the abnormal phosphorylation. In addition, recombinant protein is usually assembled in the presence of polyanionic cofactors to increase the rate [except in the case of four-repeat construct mutant K18-ΔK280 which aggregates spontaneously (*20*, *23*)]. We believe that these points are of minor consequence for the overall conformation since the resulting fibers have the same twisted appearance as Alzheimer PHFs (Figure 2), but it is possible that they contribute to the lower β-content of K19 and htau40 filaments seen by CD (Figure 4A,C).

(2) AD filament preparations created by sarkosyl extraction [preparation of Greenberg and Davies (*28*)] yield long and robust PHFs which contain tau in the pathologically phosphorylated form. Variants of this method were used by Sadqi et al. (*27*) and Berriman et al. (*32*). A problem is that these preparations may contain other protein and nonprotein components [such as fatty acids (*66*)] whose presence may distort the experimental observations, e.g., the CD curves and absorptions on which concentration estimates are based. One way to circumvent this dilemma is to "purify" individual particles by selecting them on the EM grid, as is possible with selected area diffraction (*32*), which yields unambiguous evidence of the cross-β-structure. This technique follows the general principle of X-ray fiber diffraction. The diffraction pattern from the selected area records periodic structure elements with high sensitivity, notably, the meridional peak at 0.47 nm which is characteristic of cross-β-structure.

(3) AD filaments can be isolated by immunopurification over a column containing the MC-1 antibody which recognizes a pathological conformation of tau (*30*, *31*). The main advantage is its greater purity since non-tau components are eliminated (unless they are tightly coupled to the filaments). This initial material was used both in our experiments and by Goux (*29*), although there were differences in the subsequent steps (notably, we performed an additional clearing centrifugation; see Materials and Methods).

The quantitation of secondary structure from CD and FTIR spectra is notoriously difficult; the existing examples work reasonably well in nearly "pure" cases (proteins or peptides with mostly α-helical or β-sheet structures), but quantitation remains ambiguous, especially for proteins with a largely unstructured component. The major problem is that the interpretation is based on model spectra [from peptides or proteins in defined structural states (*38*) or from crystal structures of proteins] whose applicability is uncertain in the case of natively unfolded proteins. Even in the case of well-folded proteins containing a mix of secondary structures, the standard fitting procedures cannot account for a substantial fraction of the spectra, and a range of answers can be obtained from different approaches. For example, fitting the PHF curve of K18-ΔK280 (solid line in Figure 4B) with different methods yields helix:sheet:other (coil, turn, etc.) ratios of 17:31:52 [Greenfield and Fasman (*38*)], 23:20:57 [SELCON3 (*67*)], and 22:39:39 [CONTIN (*68*, *76*)]. For the three individual Alzheimer brain-derived PHF preparations, the mean ratios of structural content are 8:18:74 (Greenfield and Fasman), 7:23:70 (SELCON3), and 13:45:42 (CONTIN). In the case of tau, the observed amplitudes of the spectra diverge considerably from the expectations based on the conventional models. For example, the CD traces of soluble tau, considered to be unfolded by the minimum around 200 nm (Figure 4), have less than half of the expected mean residue ellipticity [around -40000 deg cm^2 dmol^{-1}, Greenfield and Fasman (*38*)]. The same holds for the patterns of PHFs considered to be α-helical by their double dip at 208 and 222 nm (e.g., Figure 3 in ref *27*). These discrepancies may be explained in part by errors in the protein concentrations used to normalize the spectra. These errors are probably small for recombinant soluble tau proteins, but they could be appreciable for aggregates such as PHFs, especially when one considers possible contaminants present in Alzheimer-derived PHFs. It is notable that the spectra of reassembled PHFs (Figure 4B) and those of Alzheimer PHFs (Figure 4D) have similar shapes but differ ∼2-fold in amplitude. If one scaled up the Alzheimer PHF spectra 2-fold, the fitted α-helix content would increase from 7 to 14%, but in either case, it would remain small. The problem of quantitation becomes even more difficult for FTIR traces of largely disordered proteins. The amide I band distinguishes poorly between α-helical and random coil structure (both generate bell-shaped curves with maxima around 1650 and 1645 cm^{-1}), and the appearance of a side maximum around 1630 cm^{-1} is nonlinearly related to β-sheet structure. The amide II band is not a reliable reporter of secondary structure either because it depends on the quality of the H_2O-D_2O exchange (*69*). A similar problem with quantitation occurs with X-ray or electron diffraction which reveals the cross-β-structure of PHFs by the meridional 0.47 nm reflection even when the fraction is small (*13*, *23*, *26*, *32*).

Thus, given our limited information about the structure of disordered proteins, it seems best to base interpretations on the shapes of spectra and on salient features, rather than aiming at a strict quantitation. The approach can be validated by comparing different isoforms, constructs of domains, or mutants. For example, the fact that all forms of soluble tau (full-length isoforms or shorter constructs) are compatible with a disordered structure, as judged by various methods, is a strong indication that this disorder dominates all domains of tau, in agreement with the predictions based on structure. The fact that all PHF preparations (assembled in vitro or brain-derived) show a shift toward an increase in β-structure content, combined with the observation that the shift is most pronounced when the domains outside the repeat domain are absent, argues that the increase in β-structure content occurs predominantly in the repeat domain upon aggregation.

Despite the ambiguities of interpreting data from disordered proteins, it is clear that there are genuine discrepancies between the recent primary observations from different

authors. The CD spectra shown by Goux (*29*) show a strong dependence on buffer, interpreted as ~30% α-helix in TBS (pH 7.4) or ~40% *β*-sheet in acetate buffer (pH 6.8). We have never observed "α-helical" patterns of the kind shown by Goux from any PHF preparation, but rather patterns consistent with the mix of *β*-sheet and disordered structure [Figure 4, similar to the CD spectrum in acetate buffer (pH 6.8) published by Goux]. It is difficult to explain the source of the discrepancy, but we note that the preparation of Goux is dominated by high-molecular weight protein species whose nature is uncertain. Our preparation is dominated by the bands of the tau protein because the material was initially subjected to a clearing spin to ensure that only bona fide PHFs were used for analysis. Similar considerations apply to the study of Sadqi et al. (*27*). They claim a very high α-helix content of PHFs (~80%), based on CD and FTIR traces. As mentioned above, we cannot confirm α-helix-like CD spectra, but since the preparation based on sarkosyl insolubility is known to be heterogeneous, one can only speculate about possible contaminants (note the visible high-molecular weight contaminants). Likewise, we believe that the arguments based on the FTIR amide II band are not appropriate, and the amide I band of their PHFs in fact exhibits an additional shoulder around 1630 cm^{-1}, arguing for more *β*-structure rather than α-helix. Furthermore, the claim (in their discussion) that the combination of glycines, prolines, and serines/threonines promotes α-helical structure is, in our view, not supported by the available literature (see ref *70*), and in fact, the cited examples of fibers with high α-helix content (hemoglobin S fibers or intermediate filaments) do not support the assumption.

Overall, the data reported here are most consistent with those of Berriman et al. (*32*), who used selected area electron diffraction on PHFs derived from Down's syndrome cases by the sarkosyl solubility procedure, combined with X-ray and FTIR studies of PHFs reassembled in vitro from the P301S mutant of tau. Their diffraction data clearly highlight the cross-*β*-structure component of individual filaments (a 0.47 nm meridional reflection). For the reassembled filaments, the *β*-sheet content is quoted to be ~50% from ATR-FTIR, somewhat higher than our estimates (~20−30%) but in reasonable agreement, considering the differences in methods and preparation. Notably, no evidence of α-helix was detected by Berriman et al. (*32*), even though the preparation was comparable to that of Sadqi et al. (*27*). In summary, we conclude that PHFs are based on a core, which assumes a largely cross-*β*-conformation, while the noncore domains retain largely their unstructured state, as diagrammed in Figure 7. In this regard, our results on PHFs derived from Alzheimer brain tissue are comparable to the results for those reassembled in vitro from recombinant tau or tau mutants (*20*, *23*, *24*).

The folding principle of tau in PHFs was a matter of debate for a long time because the signature of ordered secondary structure tends to become buried in the larger disordered environment of the protein. However, the appreciation that *β*-structure is important for aggregation is only a small step toward elucidating the interaction between protein subunits. The solution will probably not come from aggregation studies of full-length tau, but from a judicious choice of small tau-derived peptides representing the assembling elements. One can take cues from recent advances in the analysis of

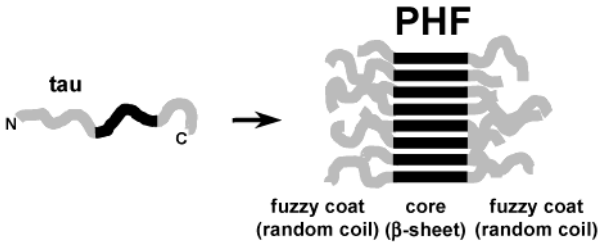

FIGURE 7: Diagram summarizing the conclusions of this study. The spectra from soluble tau are dominated by a random coil conformation (left, repeat domain in black). PHFs from AD brain or reassembled in vitro are best described by a mixture of *β*-structure and random coil structure (right). The *β*-structure is concentrated in the repeat domain, whereas the flanking domains are largely random coil. Thus, PHFs made from only short constructs containing the repeats show a greater contribution from *β*-structure than PHFs made from full-length tau.

β-amyloid, where a combination of high-resolution X-ray or EM diffraction from fibers or crystals and spectroscopic methods (EPR and solid-state NMR) has led to detailed models of the presumptive fiber core (*2*−*5*, *71*). This approach may raise concerns that the resulting fibers and prefiber oligomers are too different from those occurring in the brain, but recent evidence based on conformation-specific antibodies points to common folding states of the pathologically aggregating species (*72*). In a similar sense, one may expect that the "abnormal" conformations of tau detected by antibodies are shared by pathological monomeric, oligomeric, or fibrous states (*73*−*75*). This would provide a structural basis for identifying tau conformations or ligands, which could slow the neuronal degeneration based in tau.

ACKNOWLEDGMENT

We thank Dr. Peter Friedhoff (University of Giessen, Giessen, Germany) for help with the CD experiments, Dr. Martin von Bergen, Dr. Jacek Biernat and Dr. Eva-Maria Mandelkow (Max-Planck-Unit for Structural Molecular Biology) for many valuable suggestions, and Bianca Wichmann for excellent technical assistance.

REFERENCES

1. Glenner, G. G., Eanes, E. D., and Page, D. L. (1972) The relation of the properties of Congo red-stained amyloid fibrils to the *β*-conformation, *J. Histochem. Cytochem. 20*, 821−826.
2. Bond, J. P., Deverin, S. P., Inouye, H., El-Agnaf, O. M., Teeter, M. M., and Kirschner, D. A. (2003) Assemblies of Alzheimer's peptides Abeta25−35 and Abeta31−35: reverse-turn conformation and side-chain interactions revealed by X-ray diffraction, *J. Struct. Biol. 141*, 156−170.
3. Petkova, A. T., Ishii, Y., Balbach, J. J., Antzutkin, O. N., Leapman, R. D., Delaglio, F., and Tycko, R. (2002) A structural model for Alzheimer's beta-amyloid fibrils based on experimental constraints from solid-state NMR, *Proc. Natl. Acad. Sci. U.S.A. 99*, 16742−16747.
4. Torok, M., Milton, S., Kayed, R., Wu, P., McIntire, T., Glabe, C. G., and Langen, R. (2002) Structural and dynamic features of Alzheimer's Abeta peptide in amyloid fibrils studied by site-directed spin labeling, *J. Biol. Chem. 277*, 40810−40815.
5. Rochet, J. C., and Lansbury, P. T., Jr. (2000) Amyloid fibrillogenesis: themes and variations, *Curr. Opin. Struct. Biol. 10*, 60−68.
6. Cleveland, D. W., Hwo, S. Y., and Kirschner, M. W. (1977) Physical and chemical properties of purified tau factor and the role of tau in microtubule assembly, *J. Mol. Biol. 116*, 227−247.
7. Lee, G., Cowan, N., and Kirschner, M. (1988) The primary structure and heterogeneity of tau protein from mouse brain, *Science 239*, 285−288.

8. Schweers, O., Schonbrunn-Hanebeck, E., Marx, A., and Mandelkow, E. (1994) Structural studies of tau protein and Alzheimer paired helical filaments show no evidence for beta-structure, *J. Biol. Chem. 269*, 24290−24297.
9. Berry, R. W., Abraha, A., Lagalwar, S., LaPointe, N., Gamblin, T. C., Cryns, V. L., and Binder, L. I. (2003) Inhibition of tau polymerization by its carboxy-terminal caspase cleavage fragment, *Biochemistry 42*, 8325−8331.
10. Minoura, K., Tomoo, K., Ishida, T., Hasegawa, H., Sasaki, M., and Taniguchi, T. (2002) Amphipathic helical behavior of the third repeat fragment in the tau microtubule-binding domain, studied by (1)H NMR spectroscopy, *Biochem. Biophys. Res. Commun. 294*, 210−214.
11. Esposito, G., Viglino, P., Novak, M., and Cattaneo, A. (2000) The solution structure of the C-terminal segment of tau protein, *J. Pept. Sci. 6*, 550−559.
12. Yanagawa, H., Chung, S. H., Ogawa, Y., Sato, K., Shibata-Seki, T., Masai, J., and Ishiguro, K. (1998) Protein anatomy: C-tail region of human tau protein as a crucial structural element in Alzheimer's paired helical filament formation in vitro, *Biochemistry 37*, 1979−1988.
13. Kirschner, D. A., Abraham, C., and Selkoe, D. J. (1986) X-ray diffraction from intraneural paired helical filaments and extraneural amyloid fibers in Alzheimer disease indicates cross-β conformation, *Proc. Natl. Acad. Sci. U.S.A. 83*, 503−507.
14. Iqbal, K., Braak, H., Braak, E., and Grundke-Iqbal, I. (1993) Silver labeling of Alzheimer neurofibrillary changes and brain beta-amyloid, *J. Histotechnol. 16*, 335−342.
15. Wille, H., Drewes, G., Biernat, J., Mandelkow, E. M., and Mandelkow, E. (1992) Alzheimer-like paired helical filaments and antiparallel dimers formed from microtubule-associated protein tau in vitro, *J. Cell Biol. 118*, 573−584.
16. Goedert, M., Jakes, R., Spillantini, M. G., Hasegawa, M., Smith, M. J., and Crowther, R. A. (1996) Assembly of microtubule-associated protein tau into Alzheimer-like filaments induced by sulphated glycosaminoglycans, *Nature 383*, 550−553.
17. Perez, M., Valpuesta, J. M., Medina, M., Montejo de Garcini, E., and Avila, J. (1996) Polymerization of tau into filaments in the presence of heparin: the minimal sequence required for tau-tau interaction, *J. Neurochem. 67*, 1183−1190.
18. Kampers, T., Friedhoff, P., Biernat, J., and Mandelkow, E. M. (1996) RNA stimulates aggregation of microtubule-associated protein-tau into Alzheimer-like paired helical filaments, *FEBS Lett. 399*, 344−349.
19. Wilson, D. M., and Binder, L. I. (1995) Polymerization of microtubule-associated protein tau under near-physiological conditions, *J. Biol. Chem. 270*, 24306−24314.
20. Barghorn, S., Zheng-Fischhofer, Q., Ackmann, M., Biernat, J., von Bergen, M., and Mandelkow, E. (2000) Structure, Microtubule Interactions, and Paired Helical Filament Aggregation by Tau Mutants of Frontotemporal Dementias, *Biochemistry 39*, 11714−11721.
21. Wischik, C. M., Novak, M., Thogersen, H. C., Edwards, P. C., Runswick, M. J., Jakes, R., Walker, J. E., Milstein, C., Roth, M., and Klug, A. (1988) Isolation of a fragment of tau derived from the core of the paired helical filament of Alzheimer disease, *Proc. Natl. Acad. Sci. U.S.A. 85*, 4506−4510.
22. Novak, M., Kabat, J., and Wischik, C. M. (1993) Molecular characterization of the minimal protease resistant tau-unit of the Alzheimer's-disease paired helical filament, *EMBO J. 12*, 365−370.
23. von Bergen, M., Barghorn, S., Li, L., Marx, A., Biernat, J., Mandelkow, E. M., and Mandelkow, E. (2001) Mutations of tau protein in frontotemporal dementia promote aggregation of paired helical filaments by enhancing local beta-structure, *J. Biol. Chem. 276*, 48165−48174.
24. von Bergen, M., Friedhoff, P., Biernat, J., Heberle, J., Mandelkow, E. M., and Mandelkow, E. (2000) Assembly of tau protein into Alzheimer paired helical filaments depends on a local sequence motif ((306)VQIVYK(311)) forming beta structure, *Proc. Natl. Acad. Sci. U.S.A. 97*, 5129−5134.
25. Abraha, A., Ghoshal, N., Gamblin, T. C., Cryns, V., Berry, R. W., Kuret, J., and Binder, L. I. (2000) C-Terminal inhibition of tau assembly in vitro and in Alzheimer's disease, *J. Cell Sci. 113* (Part 21), 3737−3745.
26. Giannetti, A. M., Lindwall, G., Chau, M. F., Radeke, M. J., Feinstein, S. C., and Kohlstaedt, L. A. (2000) Fibers of tau fragments, but not full length tau, exhibit a cross beta-structure: implications for the formation of paired helical filaments, *Protein Sci. 9*, 2427−2435.
27. Sadqi, M., Hernandez, F., Pan, U., Perez, M., Schaeberle, M. D., Avila, J., and Munoz, V. (2002) Alpha-helix structure in Alzheimer's disease aggregates of tau-protein, *Biochemistry 41*, 7150−7155.
28. Greenberg, S. G., and Davies, P. (1990) A preparation of Alzheimer paired helical filaments that displays distinct tau proteins by polyacrylamide gel electrophoresis, *Proc. Natl. Acad. Sci. U.S.A. 87*, 5827−5831.
29. Goux, W. J. (2002) The conformations of filamentous and soluble tau associated with Alzheimer paired helical filaments, *Biochemistry 41*, 13798−13806.
30. Jicha, G. A., O'Donnell, A., Weaver, C., Angeletti, R., and Davies, P. (1999) Hierarchical phosphorylation of recombinant tau by the paired-helical filament-associated protein kinase is dependent on cyclic AMP-dependent protein kinase, *J. Neurochem. 72*, 214−224.
31. Vincent, I. J., and Davies, P. (1992) A protein kinase associated with paired helical filaments in Alzheimer disease, *Proc. Natl. Acad. Sci. U.S.A. 89*, 2878−2882.
32. Berriman, J., Serpell, L. C., Oberg, K. A., Fink, A. L., Goedert, M., and Crowther, R. A. (2003) Tau filaments from human brain and from in vitro assembly of recombinant protein show cross-beta structure, *Proc. Natl. Acad. Sci. U.S.A. 100*, 9034−9038.
33. Biernat, J., Mandelkow, E. M., Schröter, C., Lichtenberg-Kraag, B., Steiner, B., Berling, B., Meyer, H. E., Mercken, M., Vandermeeren, A., Goedert, M., and Mandelkow, E. (1992) The switch of tau protein to an Alzheimer-like state includes the phosphorylation of two serine-proline motifs upstream of the microtubule binding region, *EMBO J. 11*, 1593−1597.
34. Goedert, M., Wischik, C., Crowther, R., Walker, J., and Klug, A. (1988) Cloning and sequencing of the cDNA encoding a core protein of the paired helical filament of Alzheimer disease: Identification as the microtubule-associated protein tau, *Proc. Natl. Acad. Sci. U.S.A. 85*, 4051−4055.
35. Gustke, N., Trinczek, B., Biernat, J., Mandelkow, E. M., and Mandelkow, E. (1994) Domains of Tau protein and interactions with microtubules, *Biochemistry 33*, 9511−9522.
36. Friedhoff, P., Schneider, A., Mandelkow, E. M., and Mandelkow, E. (1998) Rapid assembly of Alzheimer-like paired helical filaments from microtubule-associated protein tau monitored by fluorescence in solution, *Biochemistry 37*, 10223−10230.
37. Deleage, G., Blanchet, C., and Geourjon, C. (1997) Protein structure prediction. Implications for the biologist, *Biochimie 79*, 681−686.
38. Greenfield, N., and Fasman, G. D. (1969) Computed circular dichroism spectra for the evaluation of protein conformation, *Biochemistry 8*, 4108−4116.
39. Kidd, M. (1963) Paired helical filaments in electron microscopy of Alzheimer's disease, *Nature 197*, 192−193.
40. Crowther, R. A. (1991) Straight and paired helical filaments in Alzheimer disease have a common structural unit, *Proc. Natl. Acad. Sci. U.S.A. 88*, 2288−2292.
41. Barghorn, S., and Mandelkow, E. (2002) Toward a unified scheme for the aggregation of tau into Alzheimer paired helical filaments, *Biochemistry 41*, 14885−14896.
42. Rizzu, P., Van Swieten, J. C., Joosse, M., Hasegawa, M., Stevens, M., Tibben, A., Niermeijer, M. F., Hillebrand, M., Ravid, R., Oostra, B. A., Goedert, M., van Duijn, C. M., and Heutink, P. (1999) High prevalence of mutations in the microtubule-associated protein tau in a population study of frontotemporal dementia in The Netherlands, *Am. J. Hum. Genet. 64*, 414−421.
43. Lee, V. M., Balin, B. J., Otvos, L., Jr., and Trojanowski, J. Q. (1991) A68: a major subunit of paired helical filaments and derivatized forms of normal Tau, *Science 251*, 675−678.
44. Brion, J. P., Hanger, D. P., Couck, A. M., and Anderton, B. H. (1991) A68 proteins in Alzheimer's disease are composed of several tau isoforms in a phosphorylated state which affects their electrophoretic mobilities, *Biochem. J. 279* (Part 3), 831−836.
45. Goedert, M., Spillantini, G., Cairns, N. J., and Crowther, R. A. (1992) Tau proteins of Alzheimer paired helical filaments: Abnormal phosphorylation of all six brain isoforms, *Neuron 8*, 159−168.
46. Wright, P. E., and Dyson, H. J. (1999) Intrinsically unstructured proteins: re-assessing the protein structure-function paradigm, *J. Mol. Biol. 293*, 321−331.
47. Dunker, A. K., Lawson, J. D., Brown, C. J., Williams, R. M., Romero, P., Oh, J. S., Oldfield, C. J., Campen, A. M., Ratliff, C.

M., Hipps, K. W., Ausio, J., Nissen, M. S., Reeves, R., Kang, C., Kissinger, C. R., Bailey, R. W., Griswold, M. D., Chiu, W., Garner, E. C., and Obradovic, Z. (2001) Intrinsically disordered protein, *J. Mol. Graphics Modell. 19*, 26−59.
48. Woody, R. W. (1995) Circular dichroism, *Methods Enzymol. 246*, 34−71.
49. Uversky, V. N. (2002) Natively unfolded proteins: a point where biology waits for physics, *Protein Sci. 11*, 739−756.
50. Tcherkasskaya, O., and Uversky, V. N. (2001) Denatured collapsed states in protein folding: example of apomyoglobin, *Proteins 44*, 244−254.
51. Woody, R. W., Clark, D. C., Roberts, G. C., Martin, S. R., and Bayley, P. M. (1983) Molecular flexibility in microtubule proteins: proton nuclear magnetic resonance characterization, *Biochemistry 22*, 2186−2192.
52. Brownlow, S., Morais Cabral, J. H., Cooper, R., Flower, D. R., Yewdall, S. J., Polikarpov, I., North, A. C., and Sawyer, L. (1997) Bovine beta-lactoglobulin at 1.8 Å resolution—still an enigmatic lipocalin, *Structure 5*, 481−495.
53. Chen, Y. H., Yang, J. T., and Chau, K. H. (1974) Determination of the helix and beta form of proteins in aqueous solution by circular dichroism, *Biochemistry 13*, 3350−3359.
54. Munoz, V., and Serrano, L. (1995) Analysis of i,i+5 and i,i+8 hydrophobic interactions in a helical model peptide bearing the hydrophobic staple motif, *Biochemistry 34*, 15301−15306.
55. Byler, D. M., and Susi, H. (1986) Examination of the secondary structure of proteins by deconvolved FTIR spectra, *Biopolymers 25*, 469−487.
56. Siebert, F. (1995) Infrared spectroscopy applied to biochemical and biological problems, *Methods Enzymol. 246*, 501−526.
57. Susi, H., and Byler, D. M. (1986) Resolution-enhanced Fourier transform infrared spectroscopy of enzymes, *Methods Enzymol. 130*, 290−311.
58. Surewicz, W. K., Mantsch, H. H., and Chapman, D. (1993) Determination of protein secondary structure by Fourier transform infrared spectroscopy: a critical assessment, *Biochemistry 32*, 389−394.
59. Permanne, B., Adessi, C., Saborio, G. P., Fraga, S., Frossard, M. J., Van Dorpe, J., Dewachter, I., Banks, W. A., Van Leuven, F., and Soto, C. (2002) Reduction of amyloid load and cerebral damage in a transgenic mouse model of Alzheimer's disease by treatment with a beta-sheet breaker peptide, *FASEB J. 16*, 860−862.
60. Gazit, E. (2002) A possible role for pi-stacking in the self-assembly of amyloid fibrils, *FASEB J. 16*, 77−83.
61. Hall, G. F., Lee, S., and Yao, J. (2002) Neurofibrillary degeneration can be arrested in an in vivo cellular model of human tauopathy by application of a compound which inhibits tau filament formation in vitro, *J. Mol. Neurosci. 19*, 253−260.
62. Wittmann, C. W., Wszolek, M. F., Shulman, J. M., Salvaterra, P. M., Lewis, J., Hutton, M., and Feany, M. B. (2001) Tauopathy in *Drosophila*: neurodegeneration without neurofibrillary tangles, *Science 293*, 711−714.
63. Jackson, G. R., Wiedau-Pazos, M., Sang, T. K., Wagle, N., Brown, C. A., Massachi, S., and Geschwind, D. H. (2002) Human wild-type tau interacts with wingless pathway components and produces neurofibrillary pathology in *Drosophila*, *Neuron. 34*, 509−519.
64. Kraemer, B. C., Zhang, B., Leverenz, J. B., Thomas, J. H., Trojanowski, J. Q., and Schellenberg, G. D. (2003) Neurodegeneration and defective neurotransmission in a *Caenorhabditis elegans* model of tauopathy, *Proc. Natl. Acad. Sci. U.S.A. 100*, 9980−9985.
65. Kosik, K. S., Ahn, J., Stein, R., and Yeh, L. A. (2002) Discovery of compounds that will prevent tau pathology, *J. Mol. Neurosci. 19*, 261−266.
66. Goux, W. J., Rodriguez, S., and Sparkman, D. R. (1995) Analysis of the core components of Alzheimer paired helical filaments. A gas chromatography/mass spectrometry characterization of fatty acids, carbohydrates and long-chain bases, *FEBS Lett. 366*, 81−85.
67. Sreerama, N., and Woody, R. W. (1993) A self-consistent method for the analysis of protein secondary structure from circular dichroism, *Anal. Biochem. 209*, 32−44.
68. Provencher, S. W. (1982) *Comput. Phys. Commun. 27*, 213−227.
69. Baello, B. I., Pancoska, P., and Keiderling, T. A. (2000) Enhanced prediction accuracy of protein secondary structure using hydrogen exchange Fourier transform infrared spectroscopy, *Anal. Biochem. 280*, 46−57.
70. Schulz, G. E., and Schirmer, R. H. (1997) *Principles in Protein Structure*, Springer-Verlag, New York.
71. Sikorski, P., Atkins, E. D., and Serpell, L. C. (2003) Structure and texture of fibrous crystals formed by Alzheimer's abeta(11−25) peptide fragment, *Structure 11*, 915−926.
72. Kayed, R., Head, E., Thompson, J. L., McIntire, T. M., Milton, S. C., Cotman, C. W., and Glabe, C. G. (2003) Common structure of soluble amyloid oligomers implies common mechanism of pathogenesis, *Science 300*, 486−489.
73. Jicha, G. A., Bowser, R., Kazam, I. G., and Davies, P. (1997) Alz-50 and MC-1, a new monoclonal antibody raised to paired helical filaments, recognize conformational epitopes on recombinant tau, *J. Neurosci. Res. 48*, 128−132.
74. Garcia-Sierra, F., Ghoshal, N., Quinn, B., Berry, R. W., and Binder, L. I. (2003) Conformational changes and truncation of tau protein during tangle evolution in Alzheimer's disease, *J. Alzheimer's Dis. 5*, 65−77.
75. Wolozin, B. L., Pruchnicki, A., Dickson, D. W., and Davies, P. (1986) A neuronal antigen in the brains of Alzheimer patients, *Science 232*, 648−650.
76. Provencher, S. W. (1982) *Comput. Phys. Commun. 27*, 229−242.

BI0357006